Estimation of long-term fatigue damage of fixed substructures using fully-coupled models and non-linear dynamic analysis

I. Couceiro[a,*], J. París[a], F. Navarrina[a], L. Ramírez[a], I. Colominas[a]

[a] *Group of Numerical Methods in Engineering, Civil Engineering School, Universidade da Coruña, Campus de Elviña, 15071, A Coruña, Spain*

Abstract

Typical industry models for Offshore Wind Turbines with fixed substructures are based on decoupled models between the wind turbine and the substructure. It is proved that the complete dynamic response of the structure can only be captured with coupled models. In this paper a fully-coupled model for Offshore Wind Turbines with jacket support is presented. The computational model allows to obtain an accurate response of the whole structure and the dynamic interaction between all the elements. It also allows to reproduce particular effects such as the aerodynamic damping without the need for artificial damping ratios which would be needed in decoupled models. Typical environmental offshore conditions are integrated in the model and the response of the structure is obtained by means of a non-linear time integration algorithm in order to include the effect of the continuous rotation of the blades. A cost-efficient approach for the determination of fatigue-damage in the joints of the jackets is proposed. It is based on short-time simulations which allow to accurately estimate the long-term damage in general. The estimation shows a good agreement when compared to the damage values obtained by performing the whole time-interval simulation.

Keywords: Dynamic analysis, fixed substructures, coupled models, fatigue estimation

1. Introduction

Structural analysis of offshore wind turbines (OWTs) and their substructures is one of the major challenges in offshore engineering. It is subjected to uncertainties related to loads, environmental conditions and fatigue damage assessment and there is not an agreement on how the structural model must be built. The problem is inherently dynamic and the analysis must capture the full interaction among all the elements of the OWT. Relatively long time intervals of the structural behavior need to be analyzed in order to capture the full dynamic response of the structure and the development of long-period cycles of strains and stresses (DNV-OS-J101, 2010). Additionally, the accurate representation of the offshore environmental conditions requires the consideration of a great number of different load cases. Checking the feasibility of the designs and being able to estimate the fatigue damage during the whole design life is an extremely demanding task y terms of computational resources.

Evaluating the dynamic interaction between elements is only accomplished by building coupled models where all the parts that form the OWT (substructure, tower, rotor-nacelle assembly and blades) are taken into account. However, this is not always possible since it involves larger computational effort. Traditionally, wind turbine design and substructure design are performed by different engineers and analyzed individually (Seidel, 2010). For this reason, decoupled models (where the aerodynamic calculations and effects are separated from the rest of the structure)are usually preferred (Ashish & Selvam, 2013; Ong et al., 2014; Abhinav & Saha, 2015; Lai et al., 2016; Wei et al., 2017). Hence, the masses of the blades, hub and nacelle are lumped at the top of the tower and the global resultant forces and moments are considered at the same location. A comparison of the structural responses between coupled and decoupled models can be found in (Hasselbach et al., 2013). Several discrepancies in movements, stresses and fatigue damage can be observed. One of the major drawbacks of decoupled models is the consideration of the aerodynamic damping (AD) (Kuhn, 2001; Hansen, 2015). In (Schafhirt & Muskulus, 2018) the authors compare different methods to account for aerodynamic damping in decoupled simulations calibrating them with coupled integrated analysis. The trend is significantly different for Floating Wind Turbines (FWT) where the coupled response is essential. In (Ren et al., 2015) authors propose a numerical model to capture the full dynamic response under wind and waves of a Spar-Torus combination system for a FWT. The work also addresses the long-term fatigue damage estimation of the mooring line. In (Ma et al., 2019) a coupled model is also presented for a different type of FWT. A numerical analysis of a Serbuoys-TLP platform is presented and the results are compared against experimental data.

*Corresponding author, e-mail: ivan.couceiro.aguiar@udc.es

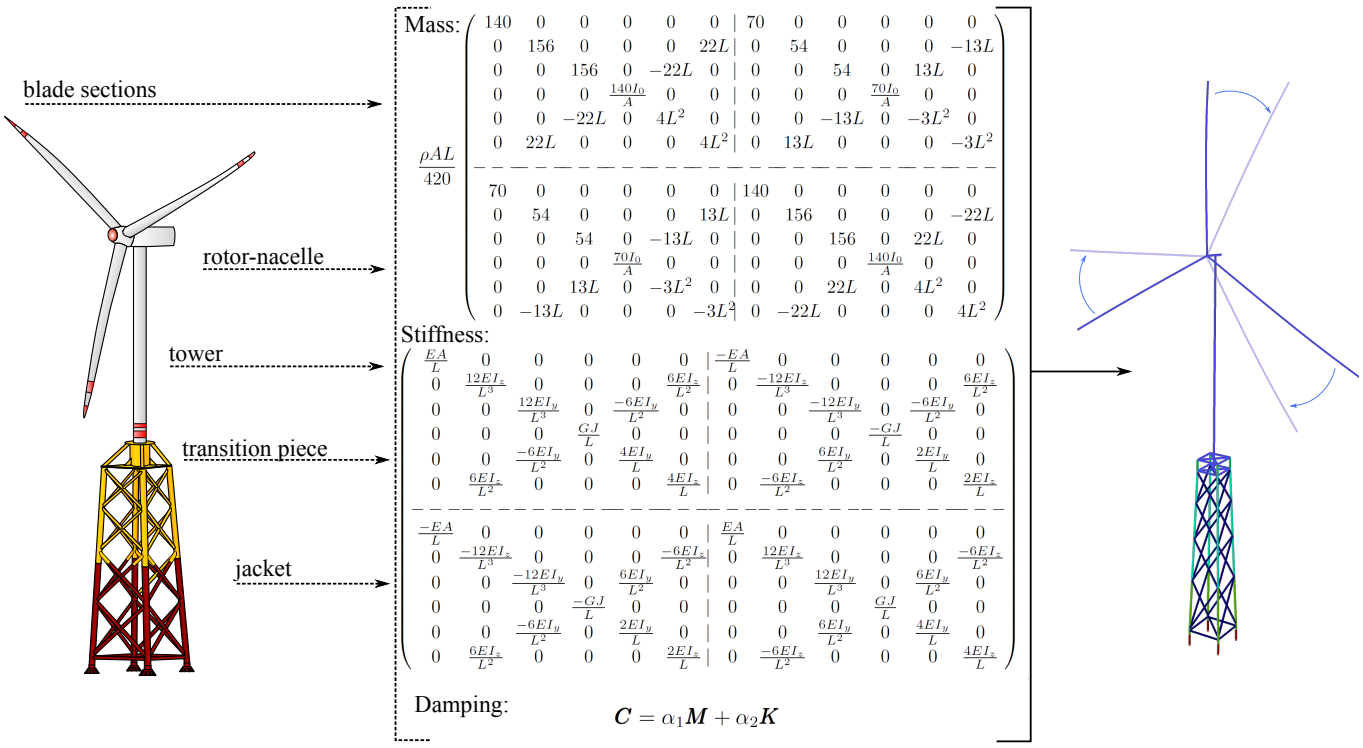

Figure 1: FEM model of the coupled OWT and condensed properties.

Dynamic analysis was traditionally used for offshore petroleum structures in the nineties (Williams et al., 1998) and generally adopted by most approaches for OWT (Elshafey et al., 2009; Raheem, 2013; Vorpahl et al., 2013; Ren et al., 2014; Passon & Branner, 2014). Nevertheless, substantial effort is devoted in an attempt to develop alternative static analysis techniques that allow to approximate the response of the structure either by quasi-static analysis, equivalent static loads (ESL) or dynamic amplification factors (DAF) (Wei et al., 2014; Gong & Chen, 2015; Chen et al., 2016). There is also a parallel trend to solve the structure in the frequency domain (Harte et al., 2012; Myers et al., 2015; Wang et al., 2017). A comparison between time domain analysis and spectral analysis can be found in (Mohammadi et al., 2016) concluding that the response at specific hot spots is highly overestimated when using spectral methods and the time domain analysis is always preferable. Typical time history analyses for the assessment of fatigue in offshore steel structures are extremely resource demanding. It must be simplified in order to increase the computational efficiency. One aforementioned approach is the analysis in the frequency domain (Yeter et al., 2015; Huang, 2017) while others seek to lighten the computing resources needed by the time history analysis by reducing the number of load cases, by lumping them into those that contribute more to fatigue (Kvittem & Moan, 2015; Zwick & Muskulus, 2015) or by using approximated approaches as Damage Equivalent Loads (DEL) (Stieng et al., 2015). An interesting approach can be found in (Dong et al., 2011) where authors fit statistical distributions of the hot-spot stresses for jacket type substructures under wind and wave conditions, what allows to quantify their contribution to the fatigue damage.

In this paper a fully coupled model for offshore wind turbines and the structural analysis of jacket type foundations considering the rotation of the blades is presented. The analysis is solved in the time domain. A non-linear integration method is used to account for the geometrical variations of the structure due to rotation. Additionally, a simplified and efficient method is proposed for the evaluation of the fatigue damage produced at the hot-spots during the whole design life of the structure.

2. Structural model and loading conditions

2.1. Structural properties and dynamics

The coupled OWT model must integrate all the individual sub-structures and their mutual interactions. In this paper, beam elements are used to model every single part of the structure. However, the turbine tower might be more accurately modeled using shell elements. Additionally the nacelle is obviously not a beam. Nevertheless, the use of more complex models for particular elements of the OWT would improve the quality of the response data only for those specific elements and not the global dynamic behavior of the structure and the dynamic interaction between elements. In the proposed model each

structural element is then determined by its mass through a consistent mass matrix $\boldsymbol{M}$(Cheng, 2001), by its stiffness through its stiffness matrix $\boldsymbol{K}$ and by a Rayleigh damping matrix $\boldsymbol{C}$ using a 2% damping ratio (ISO19902:2007, 2013). The jacket substructure used in the numerical examples is modeled using 124 elements.

The aerodynamic part of the structure used in this paper is defined in (Jonkman et al., 2009). Both, tower and blades are discretized in multiple elements with different geometrical and aerodynamic properties. Although the shape of the blade varies continuously from the rotor to the tip, the used discretized elements have constant averaged properties in their length. The weight (17.74 t) of each blade is uniformly distributed along the span. 9 different elements are used for the tower and 50 for each blade. The nacelle is also modeled by means of beam elements. The properties of each section are defined to match the mass and stiffness of the real nacelle. The hub is substituted by a 56.78 t point mass. The three-dimensional framed structure of the jacket is taken from (Vemula et al., 2010). It is a 65.65 meters high steel structure designed for a water depth of 50 m. Each element is defined by its mechanical properties. Flooded legs, marine growth and hydrodynamic added mass are considered in the model. The transition piece is a concrete block of 666 t in top of the jacket. This part is modeled by means of beam elements matching the properties of the actual piece.

2.2. Environmental loads modeling

In addition to the self weight of all structural members and buoyancy of the submerged bars of the jacket, wind and wave loads are considered in the model. Waves act on the elements under the mean sea level and the wave surface. Wind is considered acting on the tower and blades and its effect over the non-submerged part of the jacket is neglected since its influence on the structural and dynamic response of the structure is negligible in comparison with the combined effect of waves and wind on the tower and the blades.

Wind forces on the blades are usually computed with the Blade Element Momentum method (BEM). As it was mentioned before, most formulations rely on decoupled models where these forces are computed with separated aero-servo-elastic models. In this paper, forces are calculated and applied at each point of the discretized blade using its particular aerodynamic properties and wind speed at that specific location. A deep explanation for the BEM method can be found in (Burton et al., 2001; Hau, 2006; Hansen, 2015) but some details are given here for better a understanding. The wind velocity at the actuator disc U_d and its relation to the upstream velocity U_∞ can be computed using Betz's Momentum Theory as seen in figure 2. These velocities can thus be expressed as:

$$U_d = U_\infty(1 - 2\,a) \tag{1}$$

where a is the so called axial induction factor that relates the upstream velocity and the velocity at the disc. The

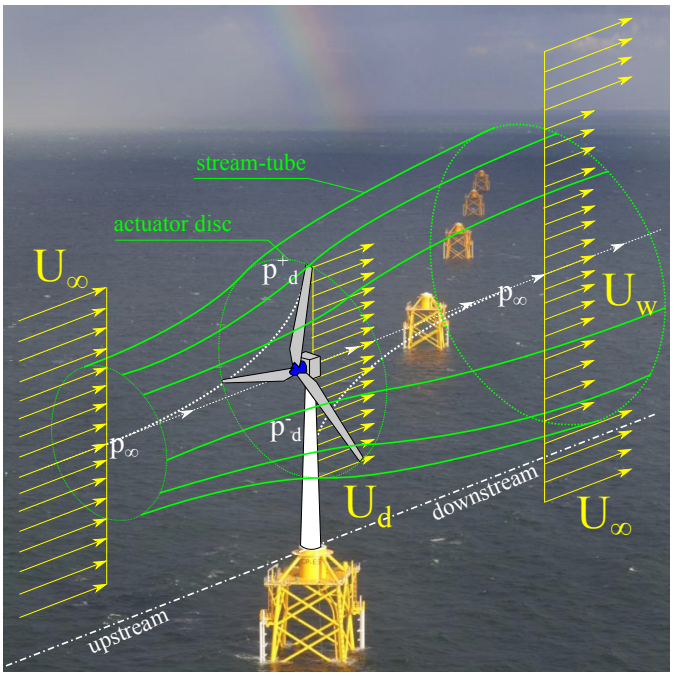

Figure 2: Stream-tube and wind velocity profiles across the actuator disc of an OWT.

pressure on the blades makes them rotate due to their aerodynamic design, converting the loss of axial momentum into the torque exerted on the rotor disc. An equal and opposite torque is then imposed on the air generating a rotating motion that is opposite to that of the blades. This change in the tangential velocity is also expressed by means of a tangential induction factor a'. The tangential velocity experienced by the blade element is then:

$$\Omega' = \Omega\, r(1 + a') \tag{2}$$

where r is the radial distance to the blade element and Ω the rotor angular speed.

The aerodynamics of the blade element are depicted in figure 3, where U_d denotes the velocity of the wind at the airfoil and R is the resultant of the flow direction on the airfoil, D and L are the drag and lift forces respectively, F_τ and F_n are the projected forces on the tangential and normal axes considering the axes of the turbine, α is the angle of attack and β is the pitch angle. Given that the induction factors are not known, we have to assume initial values and calculate the drag and lift forces according to an iterative process as:

1. Initialize $a = 0$ and $a' = 0$.
2. Using the pitch angle β and the inflow angle γ, calculate the angle of attack $\alpha = \gamma - \beta$.
3. Select the drag and lift coefficients (C_d, C_l) for the computed angle of attack and the particular airfoil section.
4. Project coefficients in normal and tangential directions:

$$\begin{aligned} C_n &= C_d \sin(\gamma) + C_l \cos(\gamma) \\ C_\tau &= -C_d \cos(\gamma) + C_l \sin(\gamma) \end{aligned} \tag{3}$$

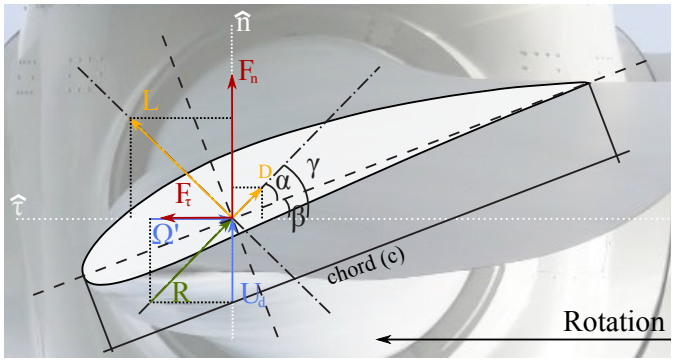

Figure 3: Velocities and forces on the blade element of an OWT.

5. Update induction factors (Hansen, 2015):

$$a = \frac{1}{\frac{4\sin^2(\gamma)F}{\sigma C_n} + 1} \quad ; \quad a' = \frac{1}{\frac{4\sin(\gamma)\cos(\gamma)F}{\sigma C_\tau} - 1} \tag{4}$$

6. Repeat from step 2 until convergence.

Expressions of (4) account for effects like the Prandtl's blade tip loss and a discrete number of blades through the tip loss factor F and the chord solidity σ (Burton et al., 2001). The above process allows to compute the tangential

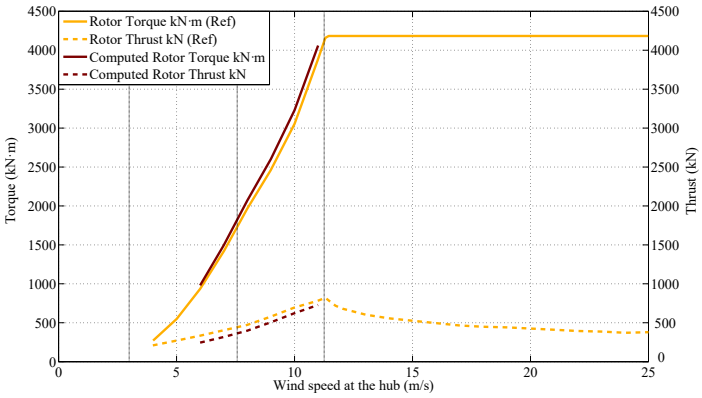

Figure 4: Total torque and thrust using the described model and the reference (Jonkman et al., 2009).

and normal force at each point of the blades. However, in up-wind mounted rotors a phenomenon called tower dam appears. The effect is a reduction of wind speed acting on the blade whenever it passes close to the tower of the OWT (Dolan & Lehn, 2006):

$$U_d' = U_d \left(1 - \frac{D_T}{2\pi} \frac{d_X}{d_X^2 + d_Y^2}\right) \tag{5}$$

where D_T is the diameter of the tower, and d_X and d_Y are the distances between the passing blade and the tower in global axes as depicted in figure 7.

The output torque and thrust using the described methodology can be compared with that of (Jonkman et al., 2009). Results are plotted in figure 4. The impact of the tower-dam effect on the total torque is shown in figure 5. On the other hand, forces due to waves on

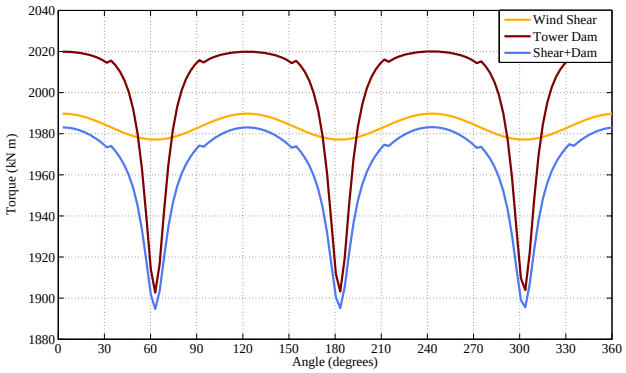

Figure 5: Total torque considering the tower-dam effect.

the jacket members are computed using Morison's formula (Morison et al., 1950) for submerged slender cylinders considering the kinematic properties of the waves given by the selected wave theory (Airy, 2nd order Stokes, 5th order Stokes) (Chakrabarti, 2005). It is worth mentioning that Morison's formula is accepted for flow perpendicular to the cylinder.

$$f_N(x,t) = \frac{\pi}{4}\rho C_M D^2 \dot{s}(x,t) + \frac{1}{2}\rho C_D D s(x,t)\,|s(x,t)| \tag{6}$$

where f_N is the perpendicular force experienced by the cylinder per unit of lenght, ρ is the water density, C_M and C_D are the inertia and drag coefficients, D is the diameter of the element and $s(x,t)$ and $\dot{s}(x,t)$ are the velocity and acceleration of the particles of the waves in the normal direction to the element.

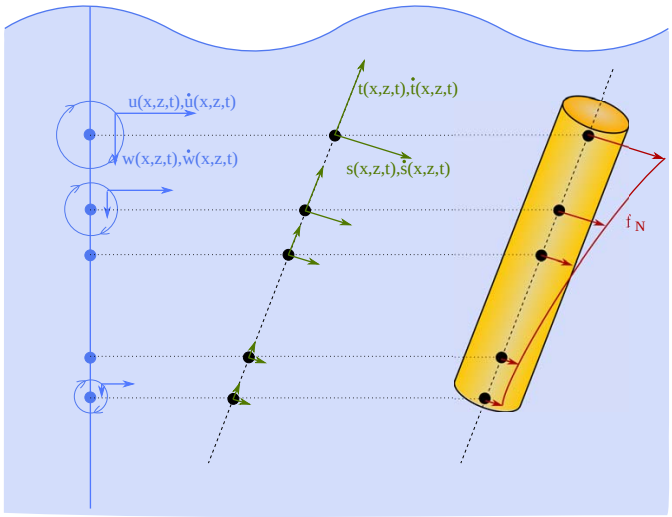

Figure 6: Simplified wave loading computation schematics

Since elements of the jacket are not normal to the waves direction of propagation, accelerations and velocities of the particles of the waves need to be projected on the local axes

of each element in order to get the two normal components with respect to the inclined submerged member. Forces due to the sea current are not accounted for but can be included in the model by modifying the particle velocities. It should be noted that in order to add the sea current velocity to the particle velocities only the component inline with the waves is used. It also alters the apparent wave period. A full description on how to include sea current in the calculations can be found in (Chakrabarti, 2005). Since the model is based on beam elements, the process of computing the wave forces at each element is as follows:

1. Discretize the element in n sub-elements.
2. Compute velocities and accelerations from waves at those discretized points in global axes (X, Y, Z).
3. Project those velocities and accelerations on the local axes of the elements (x, y, z).
4. Use Morison's formula to compute the normal forces on the element in the local y and z axes: $f'_y(x,t)$ and $f'_z(x,t)$.
5. Integrate forces along the length of the element to obtain the resultant forces F'_y and F'_z.
6. Calculate the point of application of the resultant force that will be later needed for the equivalent nodal forces and moments of the beam model.
7. Project the forces to the global axes to obtain $F_X(X,Y,Z,t)$, $F_Y(X,Y,Z,t)$ and $F_Z(X,Y,Z,t)$

Most models separate the computation of wind loads and wave loads. Commonly they are computed by using different codes and in decoupled models. In this paper, all the computations are merged in one unique model and code allowing for a complete control over all the parameters of the environment or the structure, and obtaining a direct response due to a variation of any characteristic. This allows for a direct consideration of the aerodynamic damping as explained in the following section.

3. Non-linear Time history analysis

3.1. Reference frame and integration scheme

As in any FE formulation, the model is defined under a global reference frame (X, Y, Z) whereas every element of the structure is also particularly described in a local frame (x, y, z) different for each element. However, the fully-coupled model developed, and the rotation of the blades, needs a special definition of the local reference frame. In order to maintain the principal axes of the non-axisymmetric sections of the blades, local axes y and z are defined from the axis of rotation of the turbine, in this case, global X axis ($\boldsymbol{e}_z = \boldsymbol{e}_X \times \boldsymbol{e}_x; \boldsymbol{e}_y = \boldsymbol{e}_z \times \boldsymbol{e}_x$). This guarantees that the z axis is always in the YZ plane and the orientation of the principal axis of the sections is preserved.

Since the structure is subjected to large rotations, matrices $\boldsymbol{M}$, $\boldsymbol{C}$ and $\boldsymbol{K}$ change between time-steps, and the integration of the dynamic equation ($\boldsymbol{M\ddot{u} + C\dot{u} + Ku = f}$) needs to be performed by a non-linear algorithm. In this case, displacements of the structure are solved by means of the non-linear Newmark time integration scheme.

Given the original Newmark scheme (Newmark, 1959):

$$\boldsymbol{M\ddot{u}}_{k+1} + \boldsymbol{C\dot{u}}_{k+1} + \boldsymbol{Ku}_{k+1} = \boldsymbol{f}_{k+1} \tag{7}$$

where

$$\begin{aligned} \boldsymbol{u}_{k+1} &= \boldsymbol{u}_k + \Delta t \boldsymbol{\dot{u}}_k + \frac{\Delta t^2}{2}\left[(1-2\beta)\,\boldsymbol{\ddot{u}}_k + 2\beta \boldsymbol{\ddot{u}}_{k+1}\right] \\ \boldsymbol{\dot{u}}_{k+1} &= \boldsymbol{\dot{u}}_k + \Delta t\left[(1-\gamma)\,\boldsymbol{\ddot{u}}_k + \gamma \boldsymbol{\ddot{u}}_{k+1}\right] \end{aligned} \tag{8}$$

We can define the acceleration at step $k+1$ as $\boldsymbol{\ddot{u}}_{k+1} = \boldsymbol{\ddot{u}}_k + \boldsymbol{\delta\ddot{u}}$. Then, displacements and velocities of (8) lead to:

$$\left.\begin{array}{l} \boldsymbol{u}_{k+1} = \underbrace{\boldsymbol{u}_k + \Delta t\,\boldsymbol{\dot{u}}_k + \dfrac{\Delta t^2}{2}\boldsymbol{\ddot{u}}_k}_{\boldsymbol{\widetilde{u}}_{k+1}} + \underbrace{\Delta t^2\,\beta\,\boldsymbol{\delta\ddot{u}}}_{\boldsymbol{\delta u}} \\ \\ \boldsymbol{\dot{u}}_{k+1} = \underbrace{\boldsymbol{\dot{u}}_k + \Delta t\,\boldsymbol{\ddot{u}}_k}_{\boldsymbol{\widetilde{\dot{u}}}_{k+1}} + \underbrace{\Delta t\,\gamma\,\boldsymbol{\delta\ddot{u}}}_{\boldsymbol{\delta\dot{u}}} \end{array}\right\} \Leftrightarrow \tag{9}$$

$$\Leftrightarrow \left\{\begin{array}{l} \boldsymbol{u}_{k+1} = \boldsymbol{\widetilde{u}}_{k+1} + \boldsymbol{\delta u} \\ \boldsymbol{\dot{u}}_{k+1} = \boldsymbol{\widetilde{\dot{u}}}_{k+1} + \boldsymbol{\delta\dot{u}} \end{array}\right\}$$

and the residual:

$$\boldsymbol{r} = \boldsymbol{f}_{k+1} - \boldsymbol{M\ddot{u}}_{k+1} - \boldsymbol{C\dot{u}}_{k+1} - \boldsymbol{Ku}_{k+1} \tag{10}$$

Then, Newton iterations are performed on the residual considering a linearized increment $\boldsymbol{\delta r}$ such that $\boldsymbol{r} + \boldsymbol{\delta r} = 0$, where the nonlinear contribution can be obtained as:

$$\begin{aligned} \boldsymbol{\delta r} &= \frac{\boldsymbol{\partial r}}{\boldsymbol{\partial u}}\boldsymbol{\delta u} + \frac{\boldsymbol{\partial r}}{\boldsymbol{\partial \dot{u}}}\boldsymbol{\delta\dot{u}} + \frac{\boldsymbol{\partial r}}{\boldsymbol{\partial \ddot{u}}}\boldsymbol{\delta\ddot{u}} = \\ &= \frac{\boldsymbol{\partial r}}{\boldsymbol{\partial u}}\Delta t^2\,\beta\,\boldsymbol{\delta\ddot{u}} + \frac{\boldsymbol{\partial r}}{\boldsymbol{\partial \dot{u}}}\Delta t\,\gamma\boldsymbol{\delta\ddot{u}} + \frac{\boldsymbol{\partial r}}{\boldsymbol{\partial \ddot{u}}}\boldsymbol{\delta\ddot{u}} = \\ &= \left(\Delta t^2\,\beta\,\frac{\boldsymbol{\partial r}}{\boldsymbol{\partial u}} + \Delta t\,\gamma\,\frac{\boldsymbol{\partial r}}{\boldsymbol{\partial \dot{u}}} + \frac{\boldsymbol{\partial r}}{\boldsymbol{\partial \ddot{u}}}\right)\boldsymbol{\delta\ddot{u}} \end{aligned} \tag{11}$$

From equation (10) we set that:

$$\frac{\boldsymbol{\partial r}}{\boldsymbol{\partial u}} = -\boldsymbol{K} \quad ; \quad \frac{\boldsymbol{\partial r}}{\boldsymbol{\partial \dot{u}}} = -\boldsymbol{C} \quad ; \quad \frac{\boldsymbol{\partial r}}{\boldsymbol{\partial \ddot{u}}} = -\boldsymbol{M} \tag{12}$$

And thus:

$$\boldsymbol{\delta r} = -\underbrace{\left(\Delta t^2\,\beta\,\boldsymbol{K} + \Delta t\,\gamma\,\boldsymbol{C} + \boldsymbol{M}\right)}_{\boldsymbol{K^*}}\boldsymbol{\delta\ddot{u}} \tag{13}$$

Then, solving for $\boldsymbol{r} + \boldsymbol{\delta r} = 0$, the following equation has to be solved iteratively:

$$\boldsymbol{r} = \boldsymbol{K^*}\,\boldsymbol{\delta\ddot{u}} \tag{14}$$

Figure 8 shows schematically the structural analysis of the coupled OWT. Note that at every time step the structural

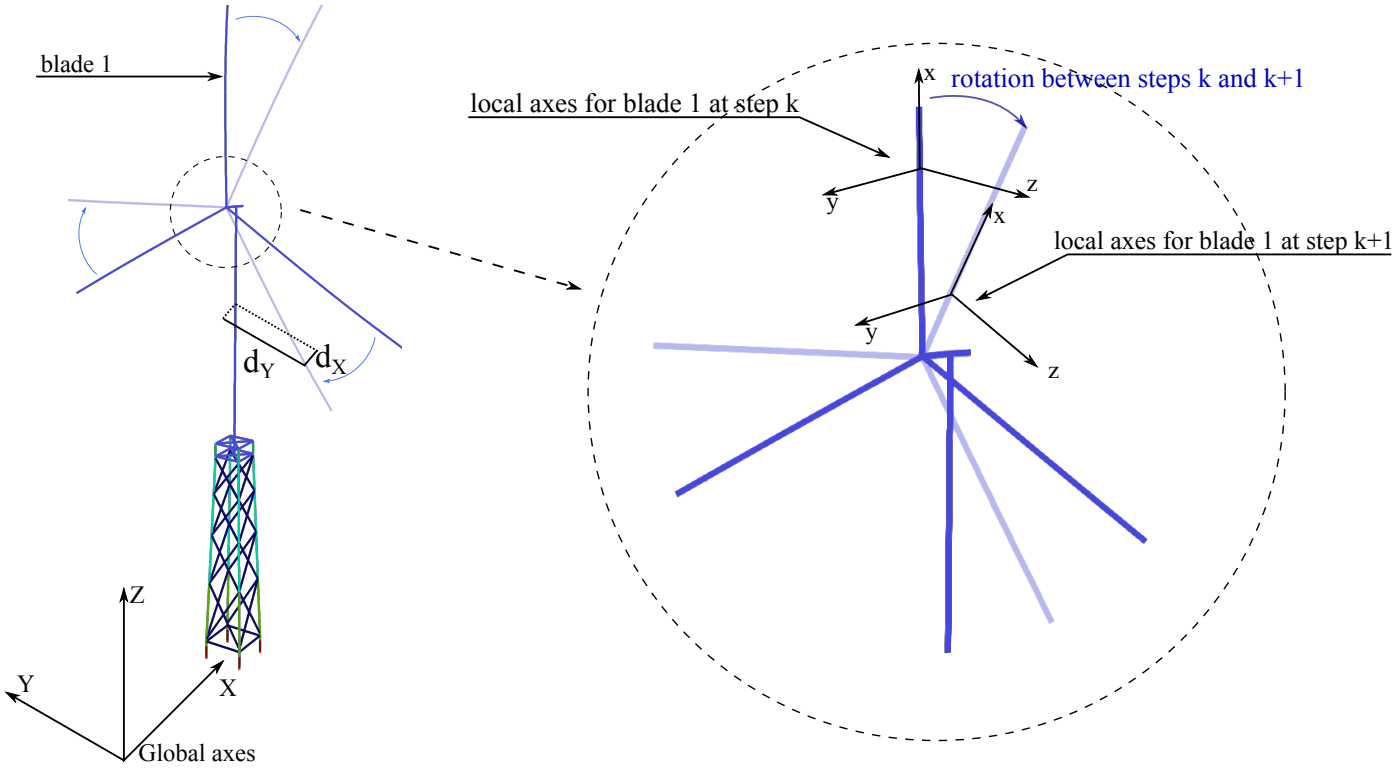

Figure 7: Definition of the global and local reference frames.

matrices need to be recalculated and thereby the whole dynamic system needs to be re-assembled. Also, since the displacements vector $\boldsymbol{u}$ involves different units of measure, movements and rotations, that can differe in their order of magnitude, typical convergence criterion may fall as they may indicate convergence because displacements dominate the norm while rotations might still be far from the right result. In this case, the convergence criteria proposed in (Chopra, 1995) and shown in the following is used:

$$\frac{(\boldsymbol{\delta r}_{k+1})^t \boldsymbol{\delta u}_{k+1}}{(\boldsymbol{r}_{k+1})^t \boldsymbol{\delta u}_k} < \varepsilon \tag{15}$$

3.2. Rotation effects and aerodynamic damping

Rotation of the blades carries several physical implications that have an impact in the way the structure and its response are accurately modeled. The most important effects would be the gyroscopic and centrifugal stiffening effect (Hamdi et al., 2014).

Centrifugal stiffening is a nonlinear effect that takes into account that the centrifugal forces acting on a rotating deformed element have a restoring effect and thus stiffen the structure. The additional stiffness can be modeled as a geometric stiffness matrix using the centrifugal force over the elements which depends on the mass, rotational speed and distance to the center of rotation. Nevertheless, both, the gyroscopic effect and the centrifugal stiffening depend directly on the speed of rotation of the elements. Thus, their influence is more acute in high speed applications and rotating machinery than in wind turbines. In fact, according to (Burton et al., 2001) changes in the first natural frequency of a single blade do not exceed 0.5%. For this reason, both effects are neglected in this work.

Figure 9 shows how the information on displacements of the blades has to be considered between time steps.

Based on the presented integration scheme, the method uses the information of displacements, velocities and accelerations at step k to obtain those at step $k+1$. Since the solution of the dynamic equation is performed in the global reference frame, displacements obtained at step k do not represent the deformed shape of the blade at step $k+1$. The deformed shape rotates along with the blade and thus displacement, velocity and acceleration vectors have to be rotated to be referred again to the global reference frame as:

$$\begin{aligned} {u'}_y^k &= u_y^k \cos(\theta_k) - u_z^k \sin(\theta_k) \\ {u'}_z^k &= u_y^k \sin(\theta_k) + u_z^k \cos(\theta_k) \end{aligned} \tag{16}$$

where, as seen in figure 9, u_y^k and u_z^k are the displacements of the blade at step k referred to global axes and ${u'}_y^k$ and ${u'}_z^k$ are the displacements obtained at step k referred to global axes with the blade at the rotated position at step $k+1$. Those displacements are the initial condition for the solution of the dynamic equation at step $k+1$.

One major advantage of fully coupled models is the direct consideration of the aerodynamic damping. Aerodynamic damping, schematically explained in figure 10, is a source of damping generated by the movement of the turbine. The wind acting on the blades generates a thrust

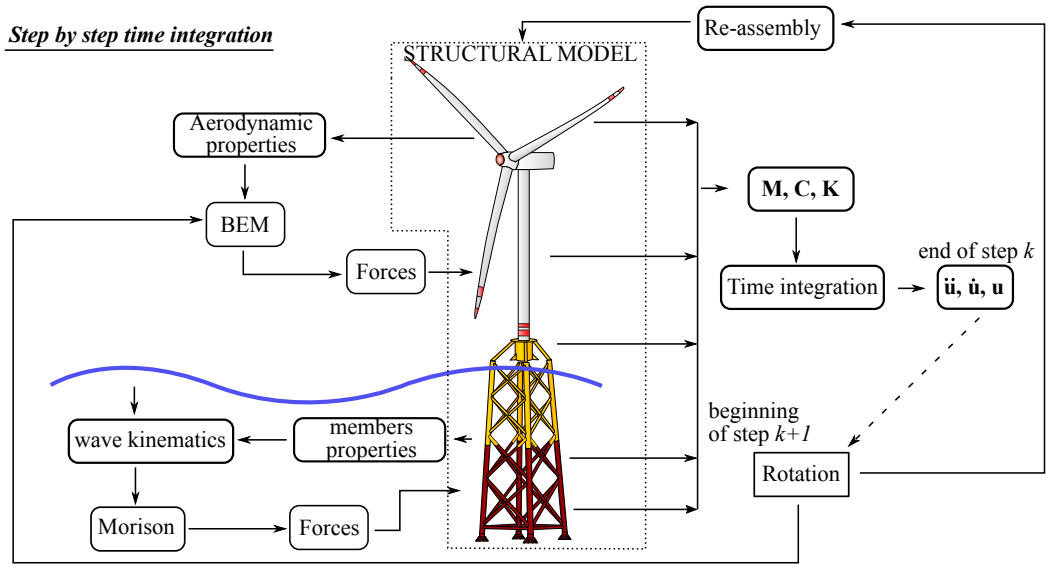

Figure 8: Structural model and coupled simulation.

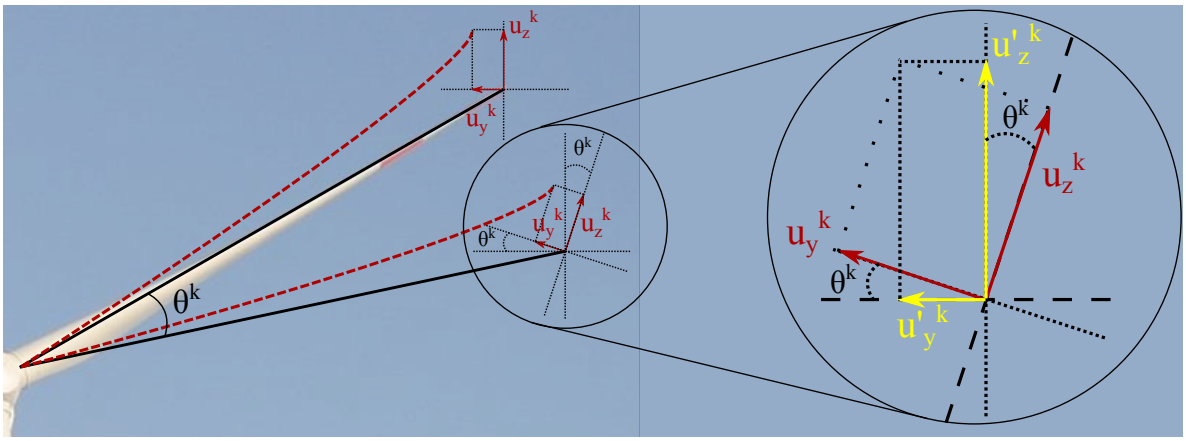

Figure 9: Displacements of the nodes of the blades referred to the local axes at step k and to local axes at step $k+1$.

force T that produces displacements u with a certain speed $\dot{u}$ and acceleration $\ddot{u}$ of those movements. Thus, the apparent speed in the wind direction experienced by the airfoil is reduced or increased by the deformation speed $\dot{u}$. Therefore, the modified apparent speed derives in a change in the angle of attack of the airfoil α. That change derives in a change in the thrust force that always works against the movement of the blade.

Consequently, the real thrust force experienced by the rotor is smaller than that considered initially. Similarly, when the blades undergo the opposite movement, the displacement speed adds to the velocity of the wind, increasing the apparent speed suffered, increasing the angle of attack, drag and lift forces and finally the thrust force. In both cases, the exerted thrust is modified by an increment or decrement of the thrust force (ΔT) that works against the motion of the blades producing a reduction of the displacements. That effect is called aerodynamic damping. Classical decoupled models introduce this phe-

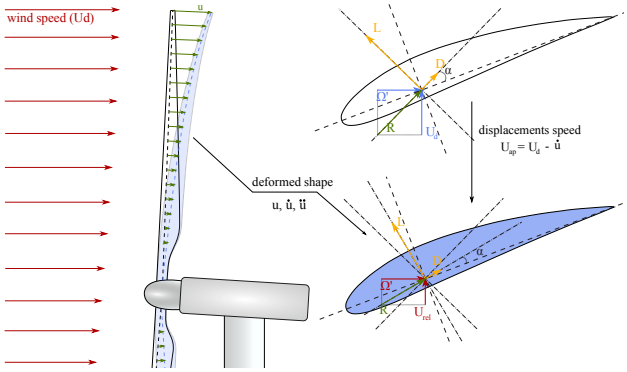

Figure 10: Modification of the relative wind speed experienced by the blades due to its deformation.

nomenon with a damping ratio coefficient ξ_{aero}. A better way to fully consider the aerodynamic damping and its impact on every section of the structure is by constructing a coupled model.

In this paper the wind speed experienced by the airfoil is modified according to the velocity of the displacements and thus, the aerodynamic damping is automatically considered. Thus, at each Newton iteration of the nonlinear Newmark integration scheme, the apparent velocity of the wind U_{ap} is recalculated with the displacement velocity of the previous iteration. Integrated coupled simulations allow to accurately obtain the response of the structure while considering the full effect of the aerodynamic damping. In (Schafhirt & Muskulus, 2018) authors present formulas to calculate the aerodynamic damping ratio needed for decoupled simulations. However it seems impossible to match every single environmental situation and the dynamic interaction produced in every possible case.

Capturing accurately the dynamic interaction between the OWT elements and the actual dynamic response is of major importance. The aerodynamic damping affects directly the amplitude of the displacements suffered by the structure, and those cyclic deformations have a severe impact on the fatigue damage produced on the support structures of the wind turbines.

4. Long-term fatigue damage assessment

Most designs of offshore steel structures are fatigue driven. Therefore, the fatigue damage experienced, specially at the welds of the joints of the frame structures, must be carefully addressed. The most extended and recommended method to calculate fatigue damage in support structures of OWT is based on the S-N curves, or Wöhler curves (DNV-RP-C203, 2011). Basically, the curves provide the fatigue limits for a given type of structure and environment based on experimental data. The limit is given as the maximum number of cycles N that the steel joint can bear until failure at a certain stress level S. In this work, the S-N approach is used and the cycles and stress ranges are obtained from the time-record of stresses using the Rainflow counting algorithm (Endo et al., 1974; ASTM-E1049-85(2011)e1, 2011). The nominal stresses obtained through the time integration and the FE formulation are scaled using Stress Concentration Factors (SCF) to account for the excessive accumulation of stresses at the joints (DNV-RP-C203, 2011). Thus, the fatigue damage of load case l is computed as:

$$D_j^l = \frac{1}{\overline{a}} \sum_{i=1}^{k} n_{i,j} \left(\frac{t_j}{t_r} \right)^{k'\, m} (\Delta\sigma_{i,j})^m \tag{17}$$

where $n_{i,j}$ and $\Delta\sigma_{i,j}$ are the number of cycles and amplitude of stresses for the hot-spot j, t_j is the thickness of the element and t_r a reference thickness. $\overline{a}$, k' and m are parameters of the S-N curves (DNV-RP-C203, 2011), k is the number of stress blocks considered representative of the stresses time-record. The parameter k should be carefully selected so that the stress range blocks do not miss any important cycle that produces a significant fatigue damage.

For a given number of load cases considered in the structure l_c, the total fatigue damage is computed as:

$$D_j^T = \sum_{l=1}^{l_c} P_l \left(\frac{1}{\overline{a}} \sum_{i=1}^{k} n_{i,j} \left(\frac{t_j}{t_r} \right)^{k'\, m} (\Delta\sigma_{i,j})^m \right) \tag{18}$$

where P_l is the probability of occurrence of load case l.

It is also important to give special care to the resolution of the stress-record given by the time-integration. The time-step Δt should also be selected such that there is not a loss of information of the stress signal. The use of a very small Δt and many range blocks k guarantees enough resolution and representation. However, those parameters should be balanced and set in accordance to the load excitation suffered by the structure and to its stress response in order to improve efficiency.

However, the main challenge in assessing fatigue damage is not how many stress blocks are sufficient nor what size of time-step is needed for enough resolution. The problem is that time-domain based fatigue computation relies upon simulating a certain time interval (usually a few minutes) of structural behavior and accumulate the damage produced in that specific window. But, in fact, what has to be guaranteed is that the damage on the joint is kept within limits during the whole design life of the structure, e.g. 20 years.

The Palmgren-Miner rule assumes that fatigue damage accumulates linearly and that it is independent from the moment of appearance. So a number of cycles of a given stress range would produce the same fatigue damage at any time of the design life (Zwick & Muskulus, 2015; Stieng & Muskulus, 2018). From that hypothesis we can build a linear extrapolation model to estimate the damage at any point of the design life from short-time simulations. The length of the simulations can not be drastically shortened. There must be a balance so the simulations are the shortest but long enough in order to allow a complete development of all the stress-cycles including high-period cycles.

In this work, the linear extrapolation proposed is build upon 300 and 600 seconds simulations. A 600 seconds simulation is run, taking an intermediate damage point at 300 s and then at the end again. Based on those two damages for each Hot-spot of the structure, the damage at any time is estimated as:

$$D_{\text{life}} = D_{300} + \frac{D_{600} - D_{300}}{300} \left(T_{\text{life}} - 300 \right) \tag{19}$$

Using the proposed extrapolation the model guarantees three basic conditions:

- The extrapolation is based on sufficient data.
- The extrapolation is based on long-enough damage recordings allowing the loads and the structural re-

sponse to be completely developed and high-period cycles are not cut out.

- The 300 and 600 seconds simulations remain on the computationally manageable window, in terms of computing time and data storage.

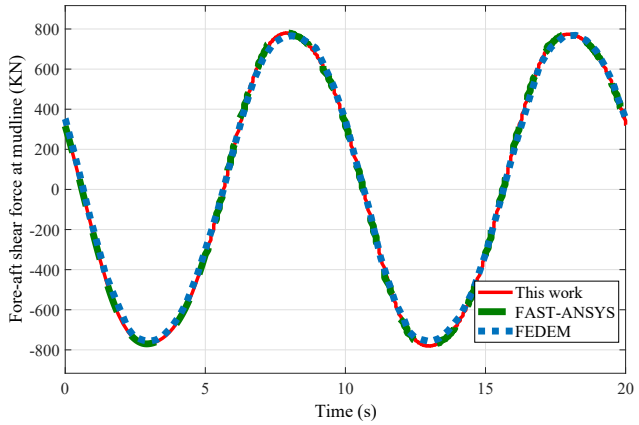

Figure 11: Comparison and verification with commercial and third party codes of computed shear force at mudline.

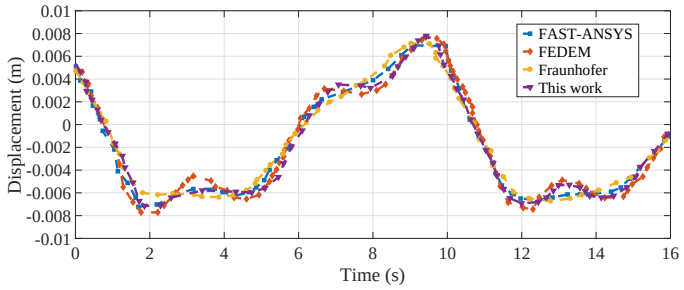

Figure 12: Comparison and verification with commercial and third party codes of computed displacements in output sensors and load cases described in (Vorpahl et al., 2012) .

5. Numerical results

Numerical results regarding the impact of the aerodynamic damping in the coupled model and the accuracy of the estimated fatigue are presented in this section. The simulation tool build in this work has been validated against the results of (Popko et al., 2014)

5.1. Jacket and OWT reference model

The UpWind reference jacket is used as model structure (Vorpahl et al., 2012). The reference completely describes the geometry and the mechanical properties of a bottom-clamped four-legged jacket. Marine growth, flooded legs and particular SCFs are considered for each specific type of joint of the jacket. A simplified transition piece consisting in a solid concrete block is used for simplicity reasons. The wind turbine model is taken from (Jonkman et al., 2009), which describes the properties of the tower, rotor-nacelle assembly, hub and the 61.5 meters blades. Each blade is divided in 50 elements and individual mechanical and aerodynamic properties are given for each section. All the properties of the model can be consulted in the cited references. The results of the proposed numerical model, including the environmental load modeling, have been tested against outputs provided in (Jonkman et al., 2009; Vorpahl et al., 2012; Popko et al., 2014). Forces and displacements fields using different loading conditions also provided in (Vorpahl et al., 2013) have been compared with the in-house code of this paper with general agreement. Figures 11 and 12 plot a comparative view for the shear force at mudline computed with the proposed model versus that computed with the FAST and FEDEM codes, and for displacements of the jacket in particular points selected as output sensors.

5.2. Aerodynamic damping

As explained in 3.2, there is a reduction in the displacements that is produced by the so called aerodynamic damping. Figure 13 shows the time-record for the displacements of the hub node in the global X axis. The plot shows the displacements obtained with the proposed model that automatically considers the aerodynamic damping vs the displacements obtained without it. In order to remove the effect of the aerodynamic damping from the model, the velocity of displacement of the blades is neglected. In both plots a test load case combining wave and wind actions has been used. For the left-hand plot wind was set to a hub-speed of 8 m/s and for the right-hand plot, up to 18 m/s. In both cases, the speed of rotation of the blades was set in accordance to the speed of the wind as exposed in (Jonkman et al., 2009). The figure shows a significant discrepancy of movements between the model with and without the aerodynamic damping. Movements for the case considering the aerodynamic damping are lower, as it was predicted.

However, the aerodynamic damping has an impact beyond the simple reduction of movements. Figure 13 also shows that not only the maximum displacements are reduced, but the shape of the dynamic response is changed. Strictly speaking, this implies a change in the number of cycles and amplitude of the stresses produced on the structure. Thus, a difference in the produced fatigue damage appears, as it can be seen in figure 14. Fatigue values are displayed separately for each type of joint, T/Y, X and K.

Figure 14 shows the resulting fatigue damage in the structure under simplified load cases. For that reason, the damage values shown are significantly below failure. For in-place real conditions the tendency is the same. The non-consideration of the aerodynamic damping in the computational model clearly augments the fatigue damage computed or estimated. Therefore, designs would be oversized. Thus, the effect of aerodynamic damping needs to be included as accurate as possible to increase the efficiency of the designs and specially for optimization purposes.

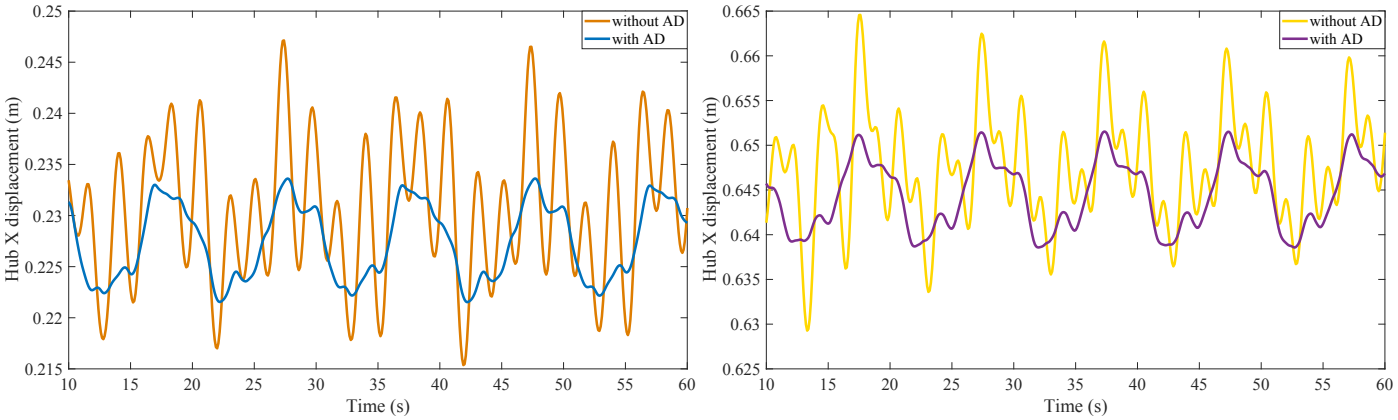

Figure 13: Comparison of hub displacement in global X axis with and without the aerodynamic damping effect for 8 m/s (left) and 18 m/s (right) of wind speed at hub.

5.3. Fatigue life prediction

In this paper a method for the estimation of long-term fatigue damage is presented. The method is based on linear extrapolation of the data collected from shorter simulations, in this case 300 and 600 seconds. This section is intended to show the accuracy of the proposed method comparing the results of the estimated damage with those obtained by simulating the whole time interval. In this case, the damage extrapolated from the 300 and 600 seconds simulation is compared to the damaged obtained simulating the full time history response of 1 year. Several load cases with waves ranging from 2 to 10 meters high and winds speeds from 2 to almost 50 m/s have been tested.

Figure 15 shows the comparison between the computed and the estimated damage for the three type of joints of the OC4 jacket. The plot shows that there is a good agreement in general between both results (computed and estimated). The average error in the estimation is only a

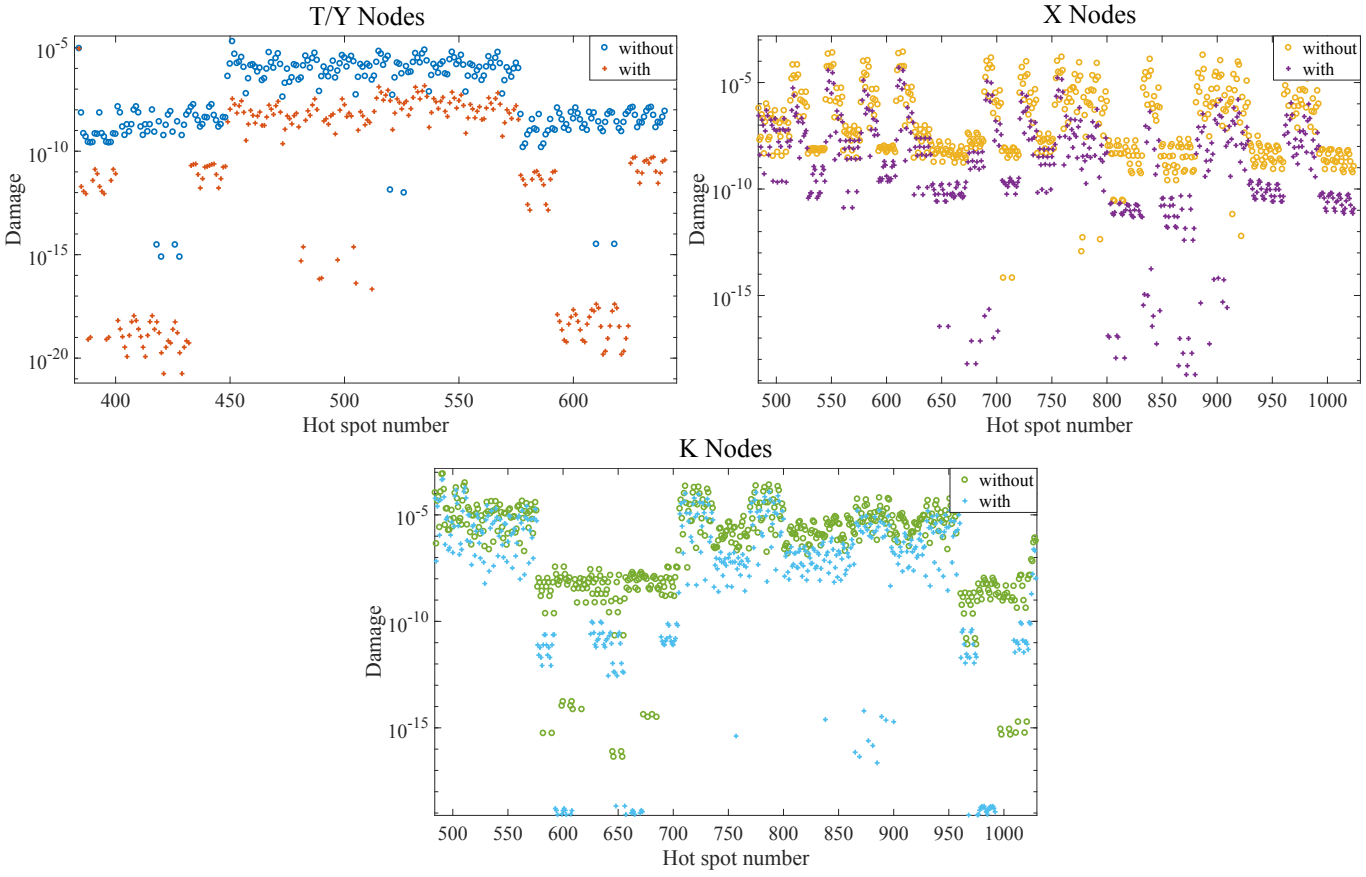

Figure 14: Fatigue damage comparison with and without the aerodynamic damping effect.

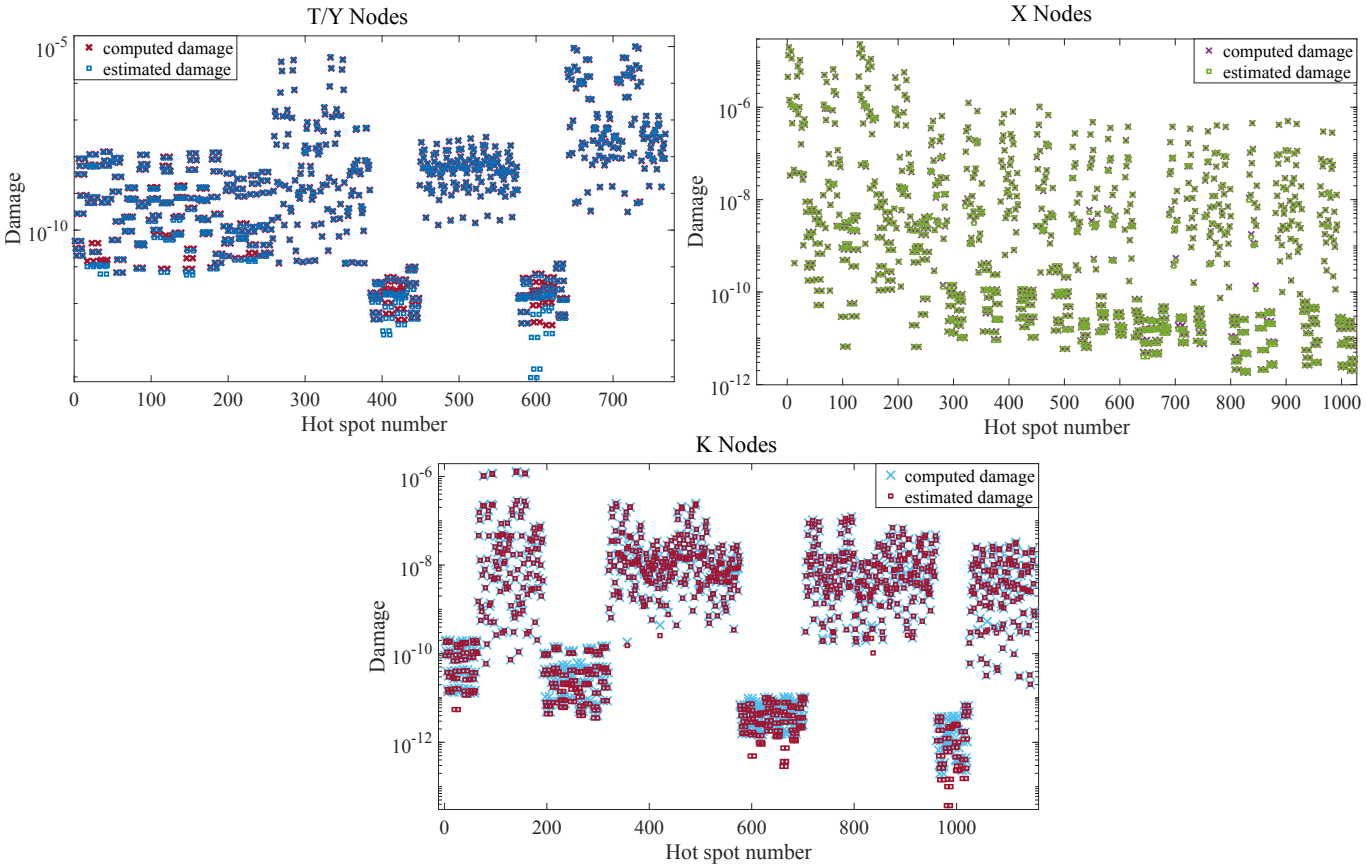

Figure 15: Comparison between the linear estimated damage and the total damage obtained by performing the simulation of the total time span.

5.26%. It is worth mention that separating the results in the three type of nodes allowed to isolate the accuracy of the estimation method for each kind of joint. It is particularly relevant that for the X type joints, the average error in the estimation was only a 0.4993%.

The methodology has been tested for different loading conditions including different wave heights and periods, different wind speeds, and variable incoming directions with similar results.

The accuracy of the estimated damage can be improved by discretely increasing the so called bin size (Li & Choung, 2017) of the rainflow counting method. The bin size defines how many divisions are taken in the cycle counting history or in other words, the level of discretization of the stress amplitudes along the stress-record. The number is related to the size of the rainflow matrix. A larger bin size means a higher precision in genera but also a higher computational cost. Current offshore standards recommend a bin size of at least 20. Figure 16 shows a box plot of the error in the estimated damage changing the bin size of the rainflow counting process between 20, 30, 40, 50 and 100. While increasing the bin size seems to reduce the error slightly, the higher the bin size the more outlier results appear. In addition that is not the only effect that can be seen in Figure 16. Error for bin sizes 30, 40 and 50 are similarly close. However, for a too-small bin size of 20 the error is higher with positive value, which means an under-estimation of the fatigue damage. However, for a too-large bin size of 100 the error is high again but with negative value, meaning an over-estimation of the fatigue damage in this case. For bin-sizes of 20 and 100 the stress-response of the structure is being over-smoothed and under-smoothed respectively. When the signal is being over-smoothed, small damaging cycles are lost. When the signal is being under-smoothed by using too-large bin sizes, noise in the signal of the stress-response is accounted for damage. From the computational point of view, the grew in the bin size did not significantly affect the CPU time. In fact, the gap between all the cases was smaller than 10 seconds while the total CPU time needed to evaluate the response and compute the damage was on the order of 10000 seconds.

6. Conclusions

In this paper, a computational model for the simulation of fully-coupled Offshore Wind Turbines with jacket foundations including all the structural elements is presented. The coupled model and the proposed non-linear time integration scheme are able to simulate the full dynamic response of the structure capturing all the possible

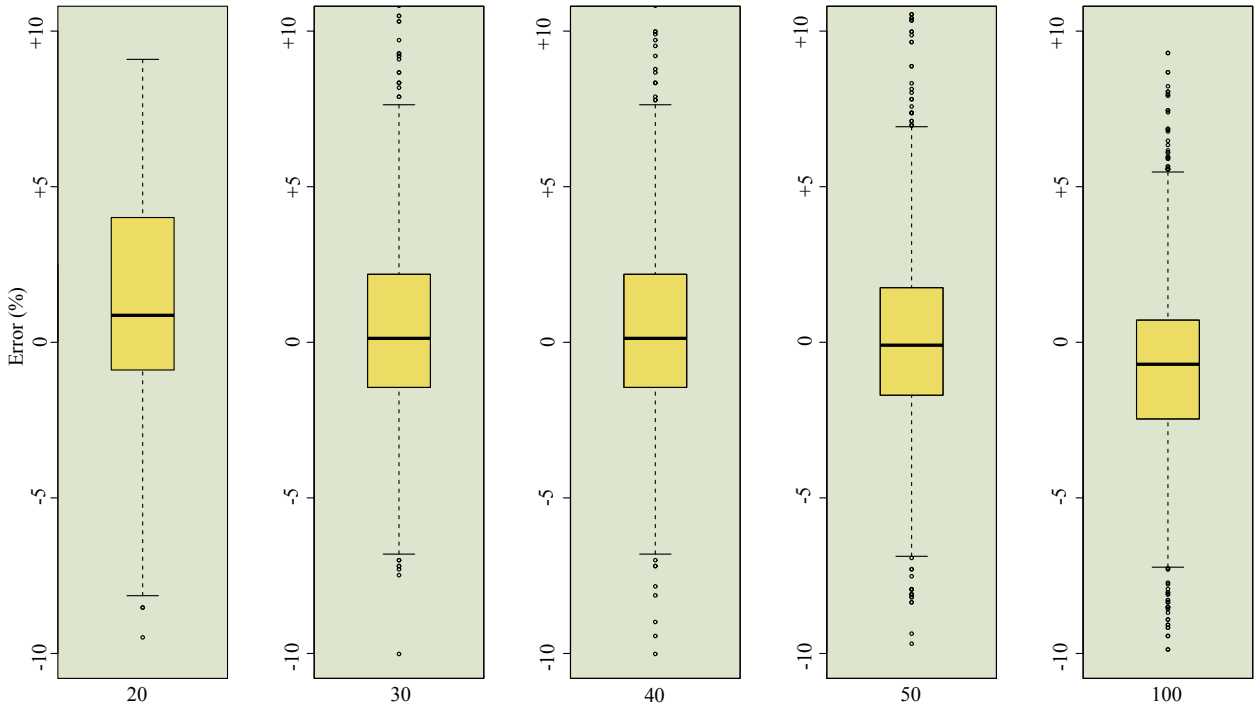

Figure 16: Error distribution of the estimated fatigue damage using different bin sizes.

dynamic interactions between the substructure, the tower of the turbine and the blades. It also allows the integration of all the environmental loads in the same computational core and the consideration of the rotation of the blades with the desired angular speed depending on the incoming wind velocity. The coupled model exposes the importance of the aerodynamic damping and the reduction in displacements experienced that can derive in a significantly different fatigue damage along time. Regarding fatigue, in this paper an estimation method for the assessment of long-term damage from short-term simulations is proposed. The results using the 300 and 600 seconds simulations are compared against full-interval simulations with good agreement of the linear extrapolation, what allows an efficient treatment of the accumulated fatigue and alleviates the computational burden of fatigue life design in real offshore structures.

acknowledgments

This work has been partially supported by FEDER funds of the European Union, by the *Ministerio de Economía y Competitividad* of the Spanish Goverment through grant # DPI2015-68431-R and grant # RTI2018-093366-B-100, by the *Secretaría Xeral de Universidades* of the *Xunta de Galicia* through grants # GRC2014/039 and # ED431C 2018/41, by the *Consellería de Cultura, Educación e Ordenación Universitaria* of the *Xunta de Galicia* by a grant awarded to the University of A Coruña, and by research fellowships of the University of A Coruña and the *Fundación de la Ingeniería Civil de Galicia*.

References

Abhinav, K. & Saha, N. (2015). Dynamic analysis of an offshore wind turbine including soil effects. In *8th International Conference on Asian and Pacific Coasts, APAC 2015* Chennai, India.

Ashish, C. & Selvam, R. P. (2013). Static and dynamic analysis of jacket substructure for offshore fixed wind turbines. In *The Eight Asia-Pacific Conference on Wind Engineering* Chennai, India.

ASTM-E1049-85(2011)e1 (2011). *Standard Practice for Cycle Counting in Fatigue Analysis*. American Society for Testing and Materials.

Burton, T., Sharpe, D., Jenkins, N., & Bossanyi, E. (2001). *Wind Energy Handbook*. John Wiley & Sons, Inc.

Chakrabarti, S. (2005). *Handbook of Offshore Engineering.*, volume 1. Elsevier.

Chen, I., Wong, B., Lin, Y., Chau, S., & Huang, H. (2016). Design and analysis of jacket substructures for offshore wind turbines. *Energies*, 9, 264.

Cheng, F. Y. (2001). *Matrix Analysis of Structural Dynamics*. Marcel Dekker, Inc.

Chopra, A. K. (1995). *Dynamics of Structures. Theory and applications to earthquake engineering*. Prentice Hall.

DNV-OS-J101 (2010). *Design of offshore wind turbine structures*. Det Norske Veritas.

DNV-RP-C203 (2011). *Fatigue design of offshore steel structures*. Det Norske Veritas.

Dolan, D. S. & Lehn, P. W. (2006). Simulation model of wind turbine 3p torque oscillations due to wind shear and tower shadow. *IEEE Transactions on Energy Conversion*, 21(3), 717–723.

Dong, W., Moan, T., & Gao, Z. (2011). Long-term fatigue analysis of multi-planar tubular joints for jacket-type offshore wind turbine in time domain. *Engineering Structures*, 33, 2002–2014.

Elshafey, A. A., Haddara, M. R., & Marzouk, H. (2009). Dynamic response of offshore jacket structures under random loads. *Marine Structures*, 22, 504–521.

Endo, T., Matsuishi, M., Mitsunaga, K., Kobayashi, K., & Takahashi, K. (1974). Rain flow method - the proposal and the applications. *Memoir Kyushu Institute Technical Engineering*.

Gong, K. & Chen, X. (2015). Improved modeling of equivalent static

loads on wind turbine towers. *Wind and Structures*, 20(5), 609–622.

Hamdi, H., Mrad, C., Hamdi, A., & Nasri, R. (2014). Dynamic response of an horizontal axis wind turbine blade under aerodynamic, gravity and gyroscopic effects. *Applied Acoustics*, 86, 154–164.

Hansen, M. O. (2015). *Aerodynamics of Wind Turbines*. Routledge.

Harte, M., Basu, B., & Nielsen, S. (2012). Dynamic analysis of wind turbines including soil-structure interaction. *Engineering Structures*, 45, 509–518.

Hasselbach, P., Natarajan, A., Jiwinangun, R., & Branner, K. (2013). Comparison of coupled and uncoupled load simulations on a jacket support structure. In *10th Deep Sea Offshore Wind R& D Conference, DeepWind'2013* Trondheim, Norway.

Hau, E. (2006). *Wind Turbines. Fundamentals, Technologies, Application, Economics*. Springer.

Huang, W. (2017). The frequency domain estimate of fatigue damage of combined load effects based on the rain-flow counting. *Marine Structures*, 52, 34–49.

ISO19902:2007 (2013). *BS EN ISO 19902:2007+A1:2013: Petroleum and natural gas industries - Fixed steel offshore structures*. British Standard.

Jonkman, J., Butterfield, S., Musial, W., & Scott, G. (2009). *Definition of a 5-MW reference wind turbine for offshore system development*. Technical report, NREL: National Renewable Energy Laboratory.

Kuhn, M. (2001). *Dynamics and design optimization of offshore wind energy conversion systems*. PhD thesis, Wind Energy Research Institute, TU Delft.

Kvittem, M. I. & Moan, T. (2015). Time domain analysis procedures for fatigue assessment of a semi-submersible wind turbine. *Marine Structures*, 40, 38–59.

Lai, W., Lin, C., Huang, C., & Lee, R. (2016). Dynamic analysis of jacket substructure for offshore wind turbine generators under extreme environmental conditions. *Applied Sciences*, 6(10), 307.

Li, C. & Choung, J. (2017). Fatigue damage analysis for a floating offshore wind turbine mooring line using the artificial neural network approach. *Ships and Offshore Structures*, 12, 288–295.

Ma, Z., Wang, S., Wang, Y., Ren, N., & Zhai, G. (2019). Experimental and numerical study on the multi-body coupling dynamic response of a novel serbuoys-tlp wind turbine. *Ocean Engineering*, 192(15), 106570.

Mohammadi, S. F., GAlgoul, N. S., Starossek, U., & Videiro, P. M. (2016). An efficient time domain fatigue analysis and its comparison to spectral fatigue assessment for an offshore jacket structure. *Marine Structures*, 49, 97–115.

Morison, J., O'Brien, M., Johnson, J., & Schaaf, S. (1950). The force exerted by surface waves on piles. *Petroleum Transactions*, 189, 149–154.

Myers, A., Arwade, S., Valamanesh, V., Hallowell, S., & Carswell, W. (2015). Strength, stiffness, resonance and the design of offshore wind turbine monopiles. *Engineering Structures*, 100, 332–341.

Newmark, N. M. (1959). A method of computation for structural dynamics. *Journal of the Engineering Mechanics Division, Proceedings of the American Society of Civil Engineers*, 1, 67–94.

Ong, M., Bachynski, E., kland, O. O., & Passano, E. (2014). Dynamic response of a jacket-type offshore wind turbine using decoupled and coupled models. In *Proceedings of the ASME 2014 33rd International Conference on Ocean, Offshore and Artic Engineering, OMAE2014* San Francisco, California, USA.

Passon, P. & Branner, K. (2014). Load calculation methods for offshore wind turbine foundations. *Ships and Offshore Structures*, 9(4), 433–449.

Popko, W., Vorphal, F., Zuga, A., Kohlmeier, M., Jonkman, J., Robertson, A., Larsen, T. J., Yde, A., Sætertrø, K., Okstad, K. M., Nichols, J., Nygaard, T. A., Gao, Z., Manolas, D., Kim, K., Yu, Q., Shi, W., Park, H., Vásquez-Rojas, A., Dubois, J., Kaufer, D., Thomassen, P., de Ruiter, M. J., van der Zee, T., Peeringa, J. M., Zhiwen, H., & von Waaden, H. (2014). Offshore code comparison collaboration continuation (oc4), phase i:results of coupled simulations of an offshore wind turbine with jacket support structure. *Journal of Ocean and Wind Energy*, 1, 1–11.

Raheem, S. E. A. (2013). Nonlinear response of fixed jacket offshore platform under structural and wave loads. *Coupled Systems Mechanics*, 2(1), 111–126.

Ren, N., Gao, Z., Moan, T., & Wan, L. (2015). Long-term performance estimation of the spar-torus-combination (stc) system with different survival modes. *Ocean Engineering*, 108(1), 716–728.

Ren, N., Li, Y., & Ou, J. (2014). Coupled wind-wave time domain analysis of floating offshore wind turbine based on computational fluid dynamics method. *Journal of Renewable and Sustainable Energy*, 6, 023106.

Schafhirt, S. & Muskulus, M. (2018). Decoupled simulatios of offshore wind turbines with reduced rotor loads and aerodynamic damping. *Wind Energy Science*, 3, 25–41.

Seidel, M. (2010). Design of support structures for offshore wind turbines - interfaces between project owner, turbine manufacturer, authorities and designer. *Stahlbau*, 79, 631–644.

Stieng, L. & Muskulus, M. (2018). Reducing the number of load cases for fatigue damage assessment of offshore wind turbine support structures using a simple severity-based sampling method. *Wind Energy Science*, 3, 805–818.

Stieng, L. E. S., Hetland, R., Schafhirt, S., & Muskulus, M. (2015). Relative assessment of fatigue loads for offshore wind turbine support structures. In *Energy Procedia. 12th Deep Sea Offshore Wind R&D Conference* Norway.

Vemula, N., DeVries, W., Fischer, T., Cordle, A., & Schmidt, B. (2010). *Design solution for the upwind reference offshore support structure*. Technical report, Rambøll, Upwind deliverable D425.

Vorpahl, F., Popko, W., & Kaufer, D. (2012). *Description of a basic model of the UpWind reference jacket for code comparison in the OC4 project under IEA Wind Annex XXX*. Technical report, Fraunhofer Institute for Wind Energy and Energy System Technology IWES.

Vorpahl, F., Schwarze, H., Fischer, T., Seidel, M., & Jonkman, J. (2013). Offshore wind turbine environment, loads, simulation, and design. *WIREs Energy Environ*, 2, 548–570.

Wang, K., Ji, C., Xue, H., & Tang, W. (2017). Frequency domain approach for the coupled analysis of floating wind turbine system. *Ships and Offshore Structures*, 12(6), 767–774.

Wei, K., Arwade, S., & Myers, A. (2014). Incremental wind-wave analysis of the structural capacity of offshore wind turbine support structures under extreme loading. *Engineering Structures*, 79, 58–69.

Wei, K., Myers, A., & Arwade, S. (2017). Dynamic effects in the response of offshore wind turbines supported by jackets under wave loading. *Engineering Structures*, 142, 36–45.

Williams, M., Thompson, R., & g.T. Houlsby (1998). Non-linear dynamic analysis of offshore jack-up units. *Computers & Structures*, 69, 171–180.

Yeter, B., Garbatov, Y., & Soares, C. G. (2015). Fatigue damage assessment of fixed offshore wind turbine tripod support structures. *Engineering Structures*, 101, 518–528.

Zwick, D. & Muskulus, M. (2015). Simplified fatigue load assessment in offshore wind turbine structural analysis. *Wind Energy*, 19(2), 265–278.